Table 1 Payload capabilities

Mission Type	Flight mode	Flights	Re-entry capsule, lb	Ascent capsule, lb	Surface cargo, lb
1) Split delivery	LOR	5	11,400	n/a	n/a
2) Split delivery	LOR	6	14,500	n/a	n/a
3) Split delivery	LDM	4	n/a	n/a	18,400
4) Split delivery	LDM	5	n/a	n/a	23,600
5) All-up delivery	LOR	8	12,100	5,500	18,100
6) All-up delivery	LOR	9	12,100	5,500	24,500

Table 2 Mission delta velocities

Mission mode	LDM, ft/s	LOR, ft/s
TLI impulsive ($C3 = -2$)	10,500	10,500
Midcourse outbound	65	65
Direct to surface impulsive	9,679	n/a
LOI	n/a	2,953
Descent	n/a	6,890
Hover	328	328
Direct to Earth ascent	9,351	n/a
Ascent to low lunar orbit	n/a	6,890
Trans-Earth injection	n/a	3,002
Midcourse inbound	65	65

burn. Results indicate that for five ETO flights of 36,400 lb each, a combination capsule of 11,400 lb can be delivered. Two of these ETO flights are propellant-transfer-only flights. (In Fig. 3, the circled numbers represent fluid transfer flights.) For six ETO flights of 36,400 lb, the payload (capsule) weight comes to 14,500 lb, and three fluid transfer flights are required.

In columns 3 and 4 of Fig. 3, under the heading LDM: CARGO ONLY, flight manifests are given for two unmanned, cargo delivery vehicles. For these missions the lander does not enter a lunar parking orbit but descends directly to the lunar surface (LDM). For four ETO flights, 18,400 lb of cargo can be delivered one way to the lunar surface. Five flights properly configured can deliver a 23,600-lb payload. These two missions utilize two stages, a translunar injection (TLI) stage and a direct to surface landing stage. In this later case (column 4) the TLI stage does a portion of the lunar deceleration burn so that the combined weight of the lander (inert), surface payload, and descent LH2 is less than the 36,400-lb launch vehicle limit. Summing up the two parts of the split-delivery approach (the crew and cargo vehicle sets), nine ETO flights are required for the two payloads of 11,400 lb (capsule) and 18,400 lb (surface module). (This is the cumulative total of columns 1 and 3.) For 11 ETO flights, a larger 14,500-lb capsule and a larger 23,600-lb surface module can be delivered (columns 2 and 4). These payload weights are also listed in Table 1, where the columns of Fig. 3 are listed as rows 1–6.

All-Up Combined Crew and Cargo

Columns 5 and 6 of Fig. 3 list the manifest for two all-up (joint crew/cargo) vehicle sets. In these cases three separate habitats are taken: a re-entry/transfer cab, a separate lander descent/ascent cab, and a large surface module. For this investigation the re-entry capsule occupied by the crew during transit was set to 12,100 lb, and the small ascent/descent-only capsule was set to 5,500 lb. (The re-entry/transit capsule is carried on the LOI/TEI stage.) For the eight ETO flight case (column 5), the surface module deliverable weight is 18,100 lb. For the nine ETO flight case this increases to 24,500 lb. (Five propellant transfer tanker flights are required for the column 5 vehicle set and six for the column 6 set.)

Notice that column 3 and 5 deliverable surface module weights are nearly equivalent (within 300 lb), as are the module weights for columns 4 and 6 (within 900 lb). This suggests that about the same amount of surface cargo can be delivered via the split-delivery approach as the all-up option at the penalty of one extra ETO flight for both the 18,000-lb and the 24,000-lb module case. That is, 9 flights (columns 1 and 3) compare with the 8 flights for the all-up case (column 5), and 10 flights for the split-delivery set (columns 1 and 4) compare with the 9 flights for the all-up case where the 24,000-lb class module is carried (column 6). Table 1 summarizes the payload capabilities listed in Fig. 3. Mission delta velocity budgets are presented in Table 2.

Reference

[1] Donahue, B., and Fowler, C., "Lunar Lander Configuration Study and Parametric Performance Analysis," AIAA Paper 93-2354, June 1993.

J. A. Martin
Associate Editor

Calculation of Pitch Damping for a Flared Projectile

N. Qin,* D. K. Ludlow,† and S. T. Shaw‡
Cranfield College of Aeronautics, Cranfield, Bedfordshire MK43 0AL, England, United Kingdom
J. A. Edwards§
Defence Research and Evaluation Agency, Fort Halstead, Sevenoaks, Kent TN14 7BP, England, United Kingdom
and
A. Dupuis¶
Defence Research Establishment (Valcartier), Courcelette, Quebec GOA 1RO, Canada

Nomenclature

C_m, C_n	= pitching and side moment coefficients, (moment)/$\frac{1}{8}\pi\rho V^2 D^3$
C_{m_q}, $C_{m_{\dot\alpha}}$	= rate of change of pitching moment with respect to q and $\dot\alpha$
D	= reference length, the projectile's diameter
M	= freestream Mach number
q	= transverse angular rate nondimensionalized by V/D
Re	= Reynolds number based on D
V	= freestream speed
x_{CG}	= distance of projectile's center of gravity from nose nondimensionalized by D
α	= angle of attack, deg
$\dot\alpha$	= rate of change of α with respect to time nondimensionalized by V/D
ρ	= freestream density
Ω	= angular rate of coning/helical motion nondimensionalized by V/D

Introduction

SCHIFF[1] has proposed to predict dynamic pitch-damping coefficients (PDCs) of bodies from steady flow computations, avoiding costly time-accurate solutions. Previously, much of this aerodynamic data was obtained from either simplified analytical approaches, empirical methods, wind-tunnel testing, or full-scale range firings. Lunar coning motion is imposed upon the projectile, and the flow-governing equations are solved in the rotating framework for which the flow is steady. Coning motion is the motion

Received Nov. 5, 1996; presented as Paper 97-0405 at the AIAA 35th Aerospace Sciences Meeting and Exhibit, Reno, NV, Jan. 6–9, 1997; revision received March 20, 1997; accepted for publication April 25, 1997.

* Senior Lecturer, Flow Control and Prediction Group. Member AIAA.
† Research Officer, Flow Control and Prediction Group.
‡ Research Assistant, Flow Control and Prediction Group.
§ Senior Principal Consultant, WX9 Department. Senior Member AIAA.
¶ Defence Scientist, Armaments Division.

performed by an object flying at a constant angle of attack with respect to the freestream velocity vector and undergoing rotation at a constant angular speed about a line parallel to the freestream flow direction passing through the projectile's center of gravity (c.g.). Use of a momentum expansion[1–3] then allows the prediction of the PDC sum ($C_{m_q} + C_{m_{\dot\alpha}}$) from static moment coefficients in the frame of reference for which the flow is steady. Some supporting experimental measurements have been performed by Schiff and Tobak.[4]

In the preceding lunar coning approach, the Magnus moment coefficient was neglected. Although this assumption is supported by experimental evidence for some cases, Magnus effects may have an important contribution to the PDC prediction. For axisymmetric bodies undergoing a coning motion with a corresponding spinning relative to the rotating framework, Weinacht et al.[5] have shown that moment expansions do not depend on Magnus effects.

It is virtually impossible to extract individual PDCs $C_{m_{\dot\alpha}}$ and C_{m_q} from free-flight aerodynamic ranges. Weinacht,[6] however, extended the use of imposed motions in a rotating framework to allow the determination of individual components of the PDC sum. This can be done by considering two different motions where the projectile's c.g. traverses a helical flight path: 1) $q = 0$ helical motion, where the body's longitudinal axis is parallel to the axis of the helix, and 2) $\dot\alpha = 0$ helical motion, where the body's longitudinal axis is tangent to its flight path.

In the present work, an implicit high-resolution parabolized Navier–Stokes (PNS) method written in a noninertial framework has been developed and used to calculate both combined and individual PDCs for a cone-cylinder-flare geometry by imposing coning, helical, and spinning motions. The PDC sum is compared with recent experimental data.

Numerical Method and Results

The governing equations are the PNS equations in a general noninertial framework, in which coning, helical, and spinning motions can be easily implemented. The present numerical method solves the PNS equations using a finite volume scheme. The convective fluxes are evaluated using Osher's approximate Riemann solver together with MUSCL interpolation and a van Albada flux limiter. Diffusive terms are discretized using central differences, with turbulence being accounted for by the Baldwin–Lomax algebraic turbulence model with the Degani–Schiff modification. A fully implicit method is employed to space-march in the streamwise direction. More details of the numerical method can be found in Ref. 7.

Recently, detailed measurements were made jointly by the Defence Research Agency and Defence Research Establishment (Valcartier) in free-flight tests for a generic cone-cylinder-flare geometry (CAN4)[8] (Fig. 1). The purpose of these tests was to provide a database of reliable experimental data against which the performance of analytical and numerical methods can be judged. The current numerical method was applied to the calculation of PDCs for the CAN4 geometry. Computations were performed for freestream Mach numbers of 4.4 and 5.725 at Reynolds numbers of 1.77×10^6 and 2.30×10^6, respectively. In both cases an angle of incidence of 2 deg was used together with an angular rate of $\Omega = 0.0045$.

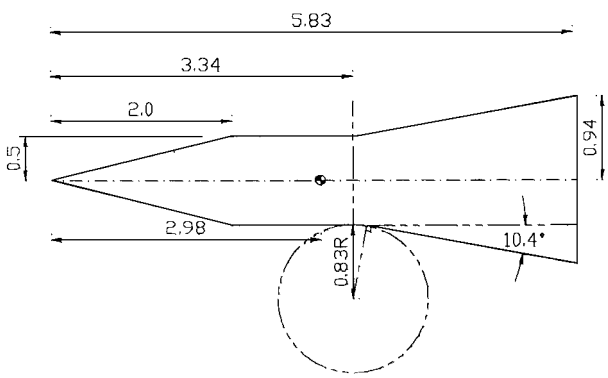

Fig. 1 CAN4 geometry; all dimensions in *D*.

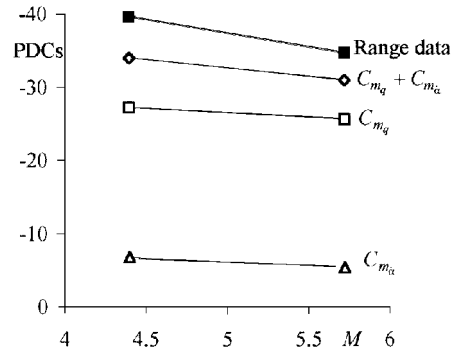

Fig. 2 Calculated PDCs for CAN4 geometry.

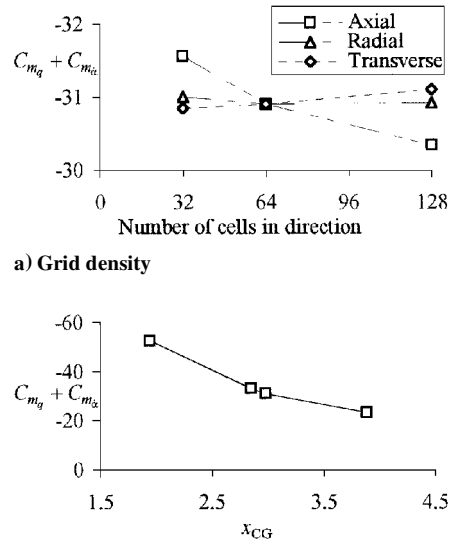

Fig. 3 Sensitivity of PDC evaluated from lunar coning motion, M = 5.725 and $Re = 2.3 \times 10^6$.

The projectile c.g. was located at a distance of $x_{CG} = 2.98$ diameters from the nose. Most of the calculations were performed on an axisymmetric grid containing 64 cells in each of the axial, radial, and transverse directions. The grid is clustered toward the body in the radial direction to ensure sufficient resolution of the boundary layer. The residual at each streamwise station was reduced by at least three orders of magnitude before the solution was considered converged.

Individual PDCs calculated from the $q = 0$ helical (with spin) and $\dot\alpha = 0$ helical motions are presented in Fig. 2; also included is a comparison of calculated and measured PDC sums. Calculations of the PDC sum using lunar coning motion or coning motion with spinning produce very similar results compared with those summed from two helical motions, which indicates that 1) the calculations using coning and helical motions are consistent and 2) the Magnus effects are small for the current problem. The present method predicts the correct trend of PDC sum with Mach number. Qualitative agreement with the range data is reasonable. However, discrepancies of about 10% are observed, possibly due to the contribution from the relatively large base area, which is not included in the current calculations.

The influence of grid resolution on PDCs obtained from lunar coning was investigated for the higher Mach number case (Fig. 3a). Generally, the calculated PDCs are not very sensitive to the grid resolution owing to the high-resolution scheme used here. Further calculations were performed to investigate the sensitivity of PDC to location of c.g. PDC sums obtained using lunar coning motion are presented in Fig. 3b, from which we observe that dramatic

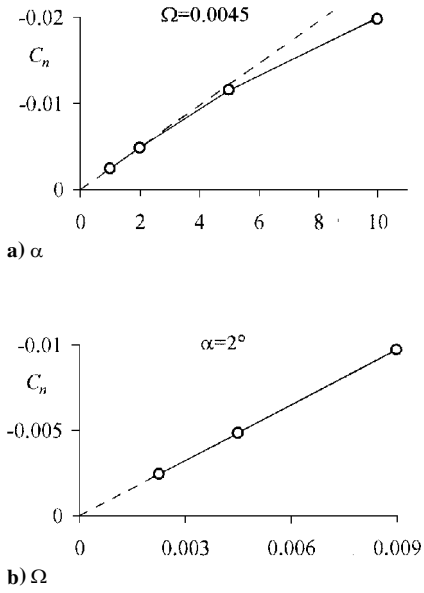

Fig. 4 Variation of side moment coefficient for CAN4 geometry undergoing lunar coning motion, $M = 5.725$ and $Re = 2.3 \times 10^6$.

changes in the PDC sum can be obtained by varying the c.g. position.

The calculation of PDCs from moment expansions is based on the assumption that forces and moments vary linearly with incidence and angular rate. The effect of angle of incidence and angular rate on the calculated side moment coefficient C_n have therefore been investigated. From Fig. 4a, it is observed that the side moment may only be considered as a linear function of incidence over a very small range of incidences below 5 deg. In Fig. 4b, side moment is seen to vary linearly with angular rate at least up to rates of 0.009. It is concluded that the parameters used in the present investigation lie within the region of linear behavior, and so the use of moment expansions is valid.

Acknowledgment

This research was supported by the Defence Research Agency under Contract WSS/V1392.

References

[1]Schiff, L. B., "A Study of the Nonlinear Aerodynamics of Bodies in Nonplanar Motion," NASA TR R-421, Jan. 1974.

[2]Murphy, C. H., "Free Flight Motion of Symmetric Missiles," U.S. Army Ballistic Research Lab., Rept. 1216, Aberdeen Proving Ground, MD, July 1963.

[3]Levy, L. L., and Tobak, M., "Nonlinear Aerodynamics of Bodies of Revolution in Free Flight," *AIAA Journal*, Vol. 8, No. 12, 1970, pp. 2168–2171.

[4]Schiff, L. B., and Tobak, M., "Results from a New Wind-Tunnel Apparatus for Studying Coning and Spinning Motions of Bodies of Revolution," *AIAA Journal*, Vol. 8, No. 11, 1970, pp. 1953–1957.

[5]Weinacht, P., Sturek, W. B., and Schiff, L. B., "Navier–Stokes Predictions of Pitch Damping for Axisymmetric Shell Using Steady Coning Motion," AIAA Paper 91-2855, Aug. 1991.

[6]Weinacht, P., "Navier–Stokes Predictions of the Individual Components of the Pitch-Damping Coefficient Sum," AIAA Paper 95-3485, Aug. 1995.

[7]Qin, N., Ludlow, D. K., Shaw, S. T., Edwards, J. A., and Dupuis, A., "Calculation of Pitch Damping Coefficients for Projectiles," AIAA Paper 97-0405, Jan. 1997.

[8]Dupuis, A., and Edwards, J. A., "Aeroballistic Range Tests of the CAN4 Projectile at Hypersonic Velocities," 21st TTCP WTP2 Meeting, Salisbury, Australia, April 1996.

R. M. Cummings
Associate Editor

Individual Components of the Yaw Damping Sum: Implementation for Tumbling Bodies

S. Ellis,* L. W. Longdon,† and G. M. Moss‡
Cranfield University, Shrivenham, Swindon SN6 8LA, Wiltshire, England, United Kingdom

Nomenclature

G	= body center of gravity
m	= mass of body
p, q, r	= components of body angular velocity about x, y, and z axes, respectively
Q	= direction of $\boldsymbol{R}$ relative to y axis in y–z plane, $\tan^{-1}(r/q)$
R'	= radius of planar loop
$\boldsymbol{R}$	= body rotation vector in y–z plane
S	= direction of $\dot{\alpha}$ relative to y axis in y–z plane
t	= time
u, v, w	= components of body linear velocity along x, y, and z axes, respectively
$\boldsymbol{V}$	= body linear velocity vector, $u\hat{\boldsymbol{\xi}} + v\hat{\boldsymbol{\eta}} + w\hat{\boldsymbol{\zeta}}$
XF, YF, ZF	= body forces in x, y, and z directions, respectively
x, y, z	= body coordinate axes
$\dot{\alpha}$	= heave component of $\mathrm{d}\sigma/\mathrm{d}t$
λ	= roll angle
$\hat{\boldsymbol{\xi}}, \hat{\boldsymbol{\eta}}, \hat{\boldsymbol{\zeta}}$	= unit vectors in x, y, and z directions, respectively
σ	= total incidence
$\boldsymbol{\omega}$	= body angular velocity vector, $p\hat{\boldsymbol{\xi}} + q\hat{\boldsymbol{\eta}} + r\hat{\boldsymbol{\zeta}}$

Subscript

e	= relative to Earth-fixed reference system

Introduction

PARTLY because of the difficulty of arriving at separate values for the individual pitch damping derivatives C_{M_q} and $C_{M_{\dot{\alpha}}}$ in external ballistic calculations, it is normal to combine the derivatives C_{M_q} and $C_{M_{\dot{\alpha}}}$ in a single term C_q (for example, Ref. 1).

Fairly recently, Weinacht[2] gave an innovative computational fluid dynamics (CFD) technique for the separate estimation of these q and $\dot{\alpha}$ dependent coefficients for a projectile in flight. That study is most likely the first time that such a predictive capability has been achieved.

If the results from such an analysis are to be useful, they need to be incorporated into an analytical model of the motion of the projectile. For normal projectile trajectory modeling, this is not strictly necessary as q and $\dot{\alpha}$ are essentially equivalent. Additionally, for linearized models, this incorporation is relatively straightforward, but the linearization process does not then make full use of the predictive potential of the CFD solutions.

This Note relates to the implementation of the separate treatment of these two motions into a full six-degree-of-freedom model, which does not contain small angle assumptions. It can therefore utilize the full potential of the CFD predictions because there are no limits on the attitude angles of the projectile. It was found that this implementation required some additional analysis; its development and use are described in this Note.

Received Jan. 2, 1997; revision received May 7, 1997; accepted for publication May 14, 1997.

*Principal Research Officer, Ballistics Group, Royal Military College of Science.

†Consultant, School of Engineering and Applied Science, Royal Military College of Science.

‡Senior Lecturer, Department of Aerospace and Guidance Systems, Royal Military College of Science.